Superplastic deformation of directionally solidified nanofibrillar Al_2O_3–$Y_3Al_5O_{12}$–ZrO_2 eutectics

José Ygnacio Pastor , Antonia Martír. , Jon M. Molina-Aldareguía , Javier LLorca
Patricia B. Oliete , Angel Larrea , José I. Peña , Victor M. Orera , Raúl. Arenal

Abstract

Nanofibrillar Al_2O_3–$Y_3Al_5O_{12}$–ZrO_2 eutectic rods were manufactured by directional solidification from the melt at high growth rates in an inert atmosphere using the laser-heated floating zone method. Under conditions of cooperative growth, the ternary eutectic presented a homogeneous microstructure, formed by bundles of single-crystal *c*-oriented Al_2O_3 and $Y_3Al_5O_{12}$ (YAG) whiskers of ≈100 nm in width with smaller Y_2O_3-doped ZrO_2 (YSZ) whiskers between them. Owing to the anisotropic fibrillar microstructure, Al_2O_3–YAG–YSZ ternary eutectics present high strength and toughness at ambient temperature while they exhibit superplastic behavior at 1600 K and above. Careful examination of the deformed samples by transmission electron microscopy did not show any evidence of dislocation activity and superplastic deformation was attributed to mass-transport by diffusion within the nanometric domains. This combination of high strength and toughness at ambient temperature together with the ability to support large deformations without failure above 1600 K is unique and shows a large potential to develop new structural materials for very high temperature structural applications.

1. Introduction

According to the second principle of thermodynamics, the efficiency of a thermal engine increases with the maximum temperature in the thermodynamic cycle. This driving force toward higher operation temperatures is currently limited by the materials' performance, as the melting point of Ni-based superalloys is below 1400 °C and oxidation becomes an issue above 1100 °C. In addition to a very high melting point, high strength and toughness are required for structural components like blades and nozzle guide vanes in gas turbines, and SiC,[1] Si_3N_4,[1] transition metal borides (ZrB_2 and HfB_2)[2] as well as SiC–C fiber composites[3] have been targeted for these applications. Nevertheless, their practical implementation was hindered by two problems. Firstly, microstructural design of high toughness ceramics normally involves the promotion of a tortuous crack path by engineering the grain boundaries or fiber-matrix interfaces. These weak links, which enhance the energy dissipation during fracture at ambient temperature, are further degraded at high temperature, dramatically reducing the creep resistance and very often resulting in brittle behavior.[1,4,5] Secondly, non-oxide ceramics are rapidly degraded by oxidation at high temperature in the aggressive environment of a combustion chamber.[6]

Directionally solidified eutectic oxides are an appealing alternative to non-oxide ceramics for high temperature structural applications as a result of their thermo-mechanical behavior.[7] In particular, they present a high melting point, excellent microstructural stability up to temperatures very close to the eutectic point, as well as chemical stability in combustion

environments.[8] This behavior is associated with an outstanding strength retention at high temperature and creep resistance due to the large area fraction of clean and strong interfaces without glassy phases, a major difference with standard ceramic oxides which present a marked degradation in strength below 1000 °C.[9,10] The best mechanical properties in terms of high temperature strength and creep resistance have been reported for Al_2O_3-based eutectics (in particular Al_2O_3–YAG, Al_2O_3–$Er_3Al_5O_{12}$ (EAG) and Al_2O_3–YAG-YSZ) with an interpenetrating microstructure[10–13] but these systems present very low toughness (in the range 2–4 MPam$^{1/2}$).[14,15] As a result, they are prone to catastrophic failure and not suitable for critical structural components within the gas turbine.

This limitation was recently overcome by ternary eutectics of the system Al_2O_3–YAG–YSZ with a nanofibrillar microstructure, which were grown by the laser-heated floating zone method at high growth rates in an inert atmosphere.[16] Under conditions of cooperative growth, the ternary eutectic presented a homogeneous microstructure, formed by bundles of single-crystal *c*-oriented Al_2O_3 and YAG whiskers of ≈100 nm in width, with smaller YSZ whiskers between them. Toughening of these materials was induced by crack deflection along the nanofibrils due to the anisotropy in the fracture toughness of sapphire and to the thermal residual stresses, leading to rods with extremely high strength (>4 GPa) and very high toughness perpendicular to the nanofibrils at ambient temperature. The high temperature properties were not explored, however, and this was the objective of this investigation.

2. Materials and experimental techniques

Ternary eutectic rods of a mixture of $Al_2O_3/Y_2O_3/ZrO_2$ were grown by directional solidification at relatively high cooling rates of 200 K/s. Ceramics were prepared using a mixture of commercial powders of Y_2O_3 (Aldrich, 99%), Al_2O_3 (Sigma–Aldrich 99.99%) and 8% yttria-stabilized zirconia (Tosoh Corporation) in the ternary (65 mol% Al_2O_3, 19 mol% ZrO_2, 16 mol% Y_2O_3) eutectic composition. Precursor rods of 2 mm in diameter and up to 100 mm in length were prepared by cold isostatic pressing for 3 min at 200 MPa followed by sintering in a furnace at 1773 K for 12 h. Eutectic rods of ≈1 mm in diameter were fabricated by directional solidification from the melt using the laser-heated floating zone method with a CO_2 laser.[10] The rods were grown in nitrogen atmosphere and the growth chamber was kept with a slight overpressure of 0.15–0.25 bar above ambient pressure in order to avoid the appearance of voids in the solidified rods. Several growth steps of diameter reduction were applied at growth rates between 100 and 250 mm/h. The last stage was always performed with the solidified rod being pulled out downwards using a growth rate of 1200 mm/h and without rotation of the crystal and precursor. A molten zone of length of ≈1.5 times the rod diameter was maintained by adjusting the laser power input.

The microstructure of the rods before and after mechanical testing was examined using TEM and SEM. For the TEM studies, thin specimens were prepared in both transverse and longitudinal cross-sections. The cross-sections were prepared by saw cutting, parallel mechanical thinning down to 40 μm and Ar^+ ion milling at 77 K, followed by carbon coating. Longitudinal and transverse cross-sections were extracted from the bent region of the rod shown in Fig. 2a using focused ion beam techniques in a Dual Beam FEI Helios 650 equipment to preserve the integrity of the sample. They were studied in a Jeol 2000FXII microscope equipped with an INCA 200 X-ray microanalysis detector. High-resolution TEM images were obtained from the longitudinal cross-sections before and after mechanical testing using a FEI Titan 60–300 kV Cube Ultra High Resolution TEM equipped with a spherical aberration objective lens corrector working at 300 kV. HRTEM images of the tested samples corresponded to the bent region of the rod. For SEM analysis, longitudinal samples of the deformed rods were cut using a diamond saw, and initially polished using diamond of 30 μm grain size as an abrasive, and afterwards with diamond slurry (up to 1 μm). The polished surfaces were coated with a thin layer of Au and observed in a field-emission SEM (Nova NanoSEM 320, FEI) using secondary and backscattered electron detectors.

The strength of the rods in the longitudinal direction was measured from 300 to 1900 K by flexure tests carried out in an alumina three-point bend testing fixture of 8.5 mm loading span. The specimen and the loading fixture were placed in a furnace and loaded through two alumina rods connected to the actuator and load cell, respectively, of a servomechanical testing machine (model 4505, Instron Ltd). The heating rate was 10 K/min up to 1300 K, 5 K/min up to 1500 K and 3 K/min up to 1700 K. The specimen was kept at the test temperature for 30 min before testing. The tests were performed in air under stroke control at a crosshead speeds in the range 10–5000 μm/min.

3. Results

The microstructure of the rods in the longitudinal and transverse direction is given in Fig. 1a and b, respectively. The component phases, α-Al_2O_3, YAG and YSZ, were identified by X-ray and electron diffraction. The Y_2O_3 content in the cubic ZrO_2 was 20 mol%, as determined by energy dispersive spectroscopy. The TEM image of the longitudinal section (Fig. 1a) shows a microstructure consisting of Al_2O_3 and YAG single-crystal whiskers up to 1 mm in length and ≈100 nm in thickness. Narrow YSZ single-crystalline fibers lay at the interfaces between sapphire and YAG. The cross-sectional microstructure as shown by the TEM image of transverse sections (Fig. 1b) shows a continuous matrix of YAG with triangular section Al_2O_3 inclusions and elongated YSZ domains at the interface. The volume composition of the material as determined from TEM images of longitudinal sections was 38, 39 and 23 vol% of Al_2O_3, YAG and YSZ respectively. The crystallographic orientations of the component phases have been previously reported.[16] Sapphire whiskers were aligned along the [0001] direction indicating a *c*-axis growth. The main growth directions of YSZ and YAG elongated domains were [0 0 1] in both cases.

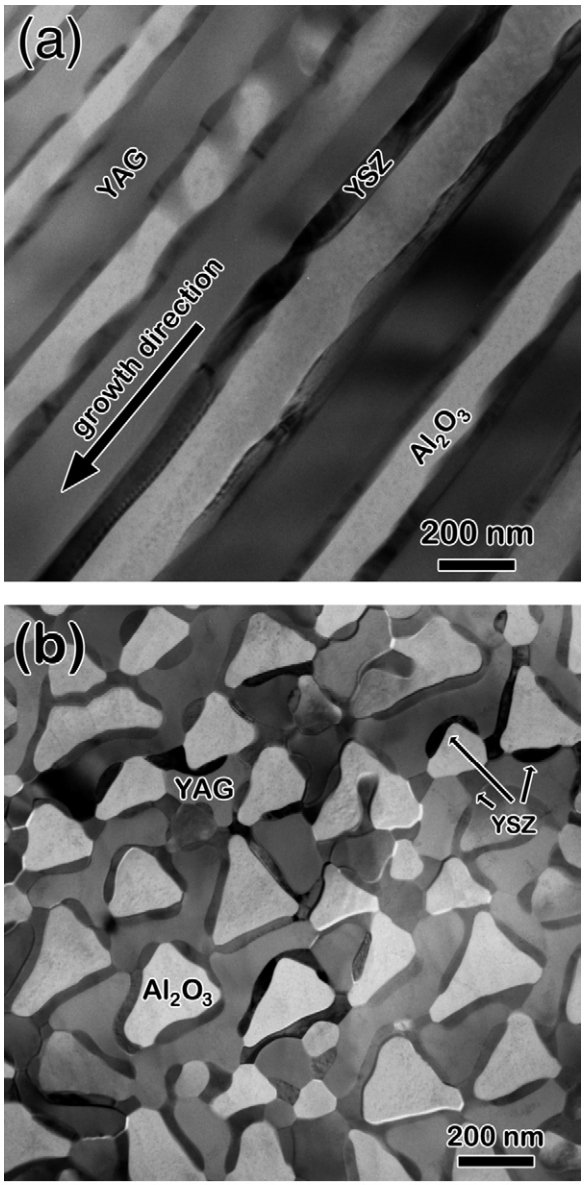

Fig. 1. TEM images showing the microstructure of the as-grown rods. (a) Longitudinal cross-section. (b) Transverse cross-section. The different phases were identified by energy dispersive spectroscopy, but can also be recognized by their gray level. In general, heavier phases appear darker in the micrograph due to higher electron scattering. The triangular shape of the Al_2O_3 inclusions observed in the transverse cross-section reflects the 3-order symmetry of the [0 0 0 1] growth axis.

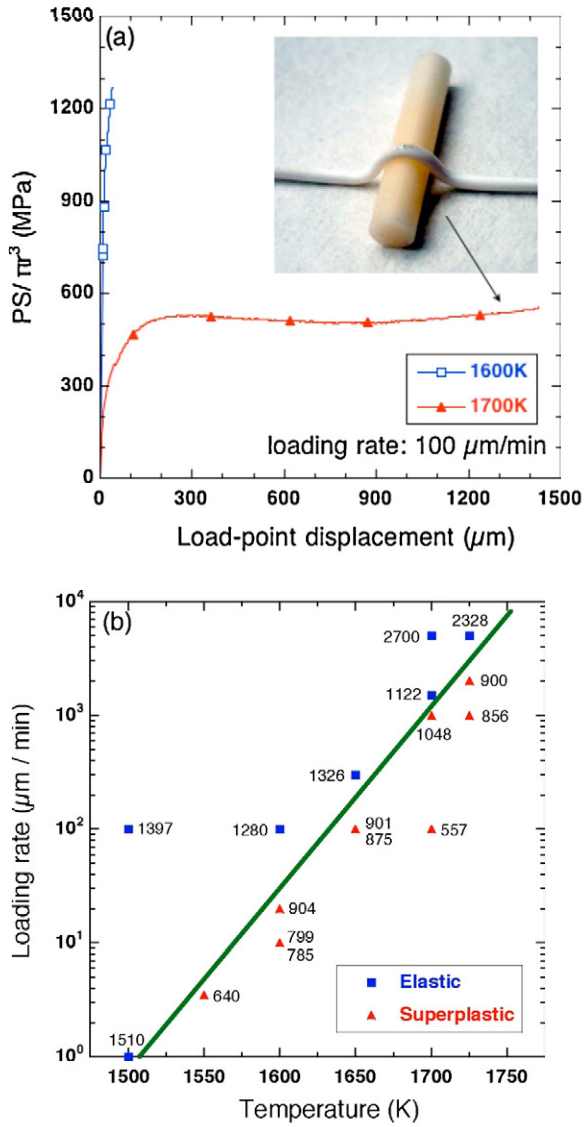

Fig. 2. (a) Representative load-displacement curves of eutectic rods displaying elastic and superplastic behavior. The inset shows the final shape of the rod, completely bent around the alumina loading after superplastic deformation. (b) Elastic and superplastic domains of deformation as a function of temperature and loading rate. The numbers indicate the bending strength (elastic) or the flow stress (superplastic).

Thermal expansion mismatch among the component phases induced thermo-elastic residual stresses upon solidification from the melt. In eutectics containing sapphire crystals, residual stresses can be accurately determined by piezospectroscopy using the shift of the Cr^{3+} ion emission present at trace level in Al_2O_3.[17] The average hydrostatic component of residual stress in the Al_2O_3 phase, measured with this technique, was -0.170 ± 0.03 GPa. This magnitude is very close to the one computed from the thermo-elastic properties of the phases using the self-consistent approximation for a three-phase composite assuming a stress-free temperature of 1493 K. Thermal expansion coefficients of Al_2O_3 and YAG are similar and close to $8 \times 10^{-6}\,K^{-1}$ but that of the minority YSZ phase is much larger: $12.65 \times 10^{-6}\,K^{-1}$. As a consequence, extremely high tensile residual stresses ($\approx$1 GPa) are expected in the YSZ phase, while Al_2O_3 and YAG are under compression.[16] The presence of such high residual stresses is in favor of strong and clean interfaces, free of glassy phases. They are normally found in eutectics grown from melt because the system has a tendency to form the most stable low-energy interfaces to minimize the system-free energy.[18]

The rods were tested under three-point bending at temperatures in the range 1500–1700 K at different strain rates, as defined by the crosshead speed. Two different behaviors were found, as depicted in Fig. 2a. At low temperature and high strain rate, the mechanical behavior was practically linear until

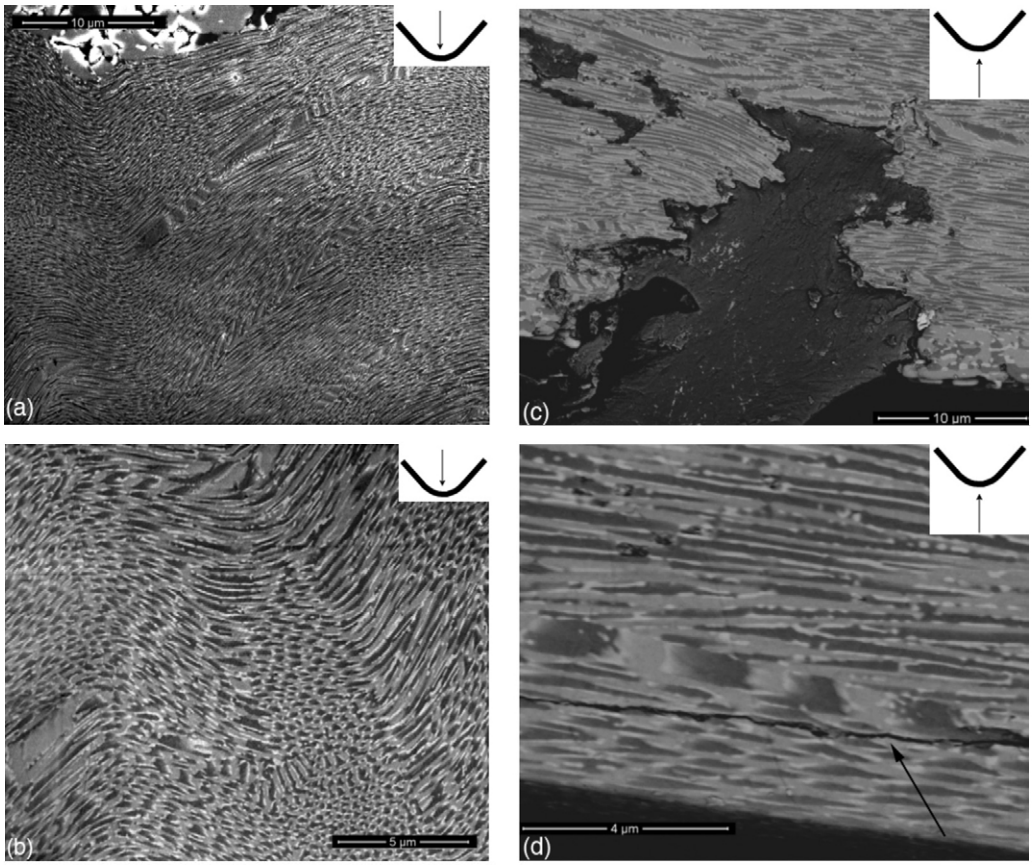

Fig. 3. SEM micrographs of the longitudinal section of a rod after superplastic deformation. (a) Secondary electron micrograph showing significant distortion of the microstructure below the loading point due to plastic deformation. (b) Back-scattered electron detail of (a). Contrary to TEM images, Al_2O_3 appears black, YAG gray and YSZ white. (c) Back-scattered electron micrograph of a surface defect at the tensile region of the rod. (d) Idem as (c), showing the propagation of a crack (marked with an arrow) from the defect parallel to the rod axis.

fracture, in agreement with the standard behavior of ceramic eutectics. The bending strength could be determined from maximum load, P_{max}, following the strength of materials theory for a Bernoulli elastic beam of circular section according to $\sigma_b = P_{max} S/\pi r^3$, where S is the span and r the rod radius. The bending strength of the elastic rods can be found in Fig. 2b for different temperatures and loading rates. These values are lower than those measured previously at ambient temperature (>4 GPa)[16] but equivalent to those reported in the same temperature range for ternary $Al_2O_3/Y_2O_3/ZrO_2$ eutectics with micron or submicron domains arranged in a three-dimensional interpenetrating network.[19,20]

Surprisingly, the typical elastic behavior until fracture of these eutectics changes abruptly at higher temperatures and/or lower loading rates to a ductile regime in which the rods underwent very large plastic deformations without fracture. An extreme, but representative, case is found in the inset of Fig. 2a, where the eutectic rod is completely bent around the alumina loading pin. If all the tests are represented in a loading rate *vs.* temperature diagram (Fig. 2b), two different regions appear: elastic behavior is found in the upper-left region, which corresponds to low temperature/high strain rates, while superplastic deformation is concentrated in the lower-right zone. It should be noted that superplastic deformation occurred at a constant flow stress that depended on temperature and loading rate (Fig. 2b).

The fracture and deformation mechanisms of the elastic and superplastic samples were studied by scanning electron microscopy (SEM). Elastic rods failed with the propagation of a brittle crack from surface defects, in agreement with previous observations in these ternary eutectics.[19,20] Superplastic samples were not broken and the microstructure of the rods was analyzed just below the loading point (Fig. 3a and b) where the rod underwent the largest (compressive) stresses and at the opposite surface (Fig. 3c), where the tensile stresses were maximum. The secondary and back-scattered electron images just below the loading point showed that the fibrillar microstructure had become wavy. Neither cracks nor other defects were found, indicating that all the phases were able to accommodate the large plastic strains. On the contrary, surface defects were found in the tensile region of the rod, as shown in Fig. 3c. These defects did not lead, however, to fracture by the propagation of a crack perpendicular to the rod axis. On the contrary, the cracks propagated parallel to the rod (Fig. 3d) and did not cause brittle fracture. This mechanism of toughening by crack deflection was already found at ambient temperature and it was responsible for the extremely high bending strength of the rod.[16] Crack deflection in the nanofibrillar eutectic was attributed to two cooperative mechanisms at ambient temperature, namely the thermal residual stresses and the anisotropy of the fracture toughness of sapphire. These results indicate

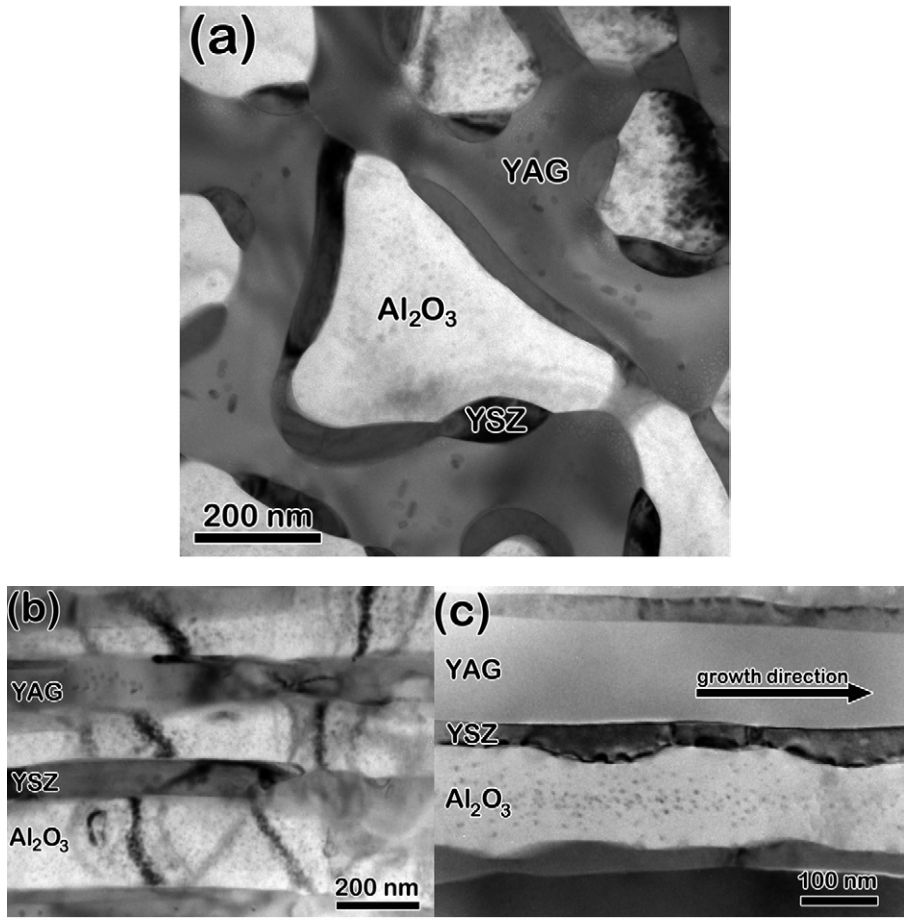

Fig. 4. TEM images obtained from transverse (a) and longitudinal (b) cross-sections of the deformed and of the longitudinal (c) cross-section of the non-deformed region of the ternary eutectic rod. The rod growth direction was horizontal in both cases, as shown in (c). Neither dislocations nor interphase amorphous precipitates were found in either region. The image (b) shows the presence of bend contours, mainly evident in the alumina phase, associated to the macroscopic superplastic deformation of the sample. The small precipitates in both Al_2O_3 and YAG (although the density is higher in Al_2O_3) are attributed to vacancy aggregation.

that the differences in the toughness of sapphire between the basal (0 0 0 1) plane (4.5 MPam$^{1/2}$) and the prismatic (11–20) or rhombohedral (10–12) planes (2.4 MPam$^{1/2}$)[21] is sufficient to promote crack deflection in this nanofibrillar microstructure.

In order to gain understanding of the physical mechanisms responsible for the superplastic behavior, transmission electron microscopy (TEM) samples were obtained from the deformed region below the loading point. Samples from the non-deformed areas of the same superplastic rod were also examined. Precipitates of ~10 nm were abundantly found in the alumina phase in both deformed and non-deformed zones (Fig. 4). They showed a coffee bean type contrast that is typically attributed to coherent precipitates probably formed by aggregation of vacancies during heating. Slightly larger precipitates (≈15 nm) were also found in YAG but the density was lower.

HRTEM was carried out in order to ascertain the presence of amorphous precipitates or glassy zones at the interfaces before or after deformation. The HRTEM images of the three interfaces, Al_2O_3–YAG, Al_2O_3–YSZ and YAG–YSZ, corresponding to the as-processed ternary eutectic are shown in Fig. 5a–c, respectively. Similar HRTEM images were obtained from the region deformed superplastically in the bent rods and are shown in Fig. 6. Both figures, representative of the interfaces in the ternary eutectic, demonstrate that neither amorphous precipitates nor glassy zones were present in the ternary eutectic before or after deformation. This feature, which hinders the activation of domain boundary sliding as the dominant deformation mechanisms, is a well-known characteristic of directionally solidified eutectics, responsible for their excellent creep resistance.[9,13,14,22–24]

In addition, dislocations were not found in the deformed region. As the rods were highly textured, the absence of dislocations was checked in both transverse and longitudinal cross-sections and under various electron illumination conditions. The only feature associated with the deformation observed in the TEM analysis was the presence of bend contours, mainly in the alumina phase (Fig. 4b). These contours are formed by diffraction of crystallographic planes that rock into the Bragg condition due to the macroscopic bending of the specimen. The presence of these contours is in agreement with the large deformations undergone by the nanofibrillar crystals under the loading points, as shown by SEM (Fig. 3a and b). Note also that the contours of Fig. 4b were perpendicular to the deformation axis.

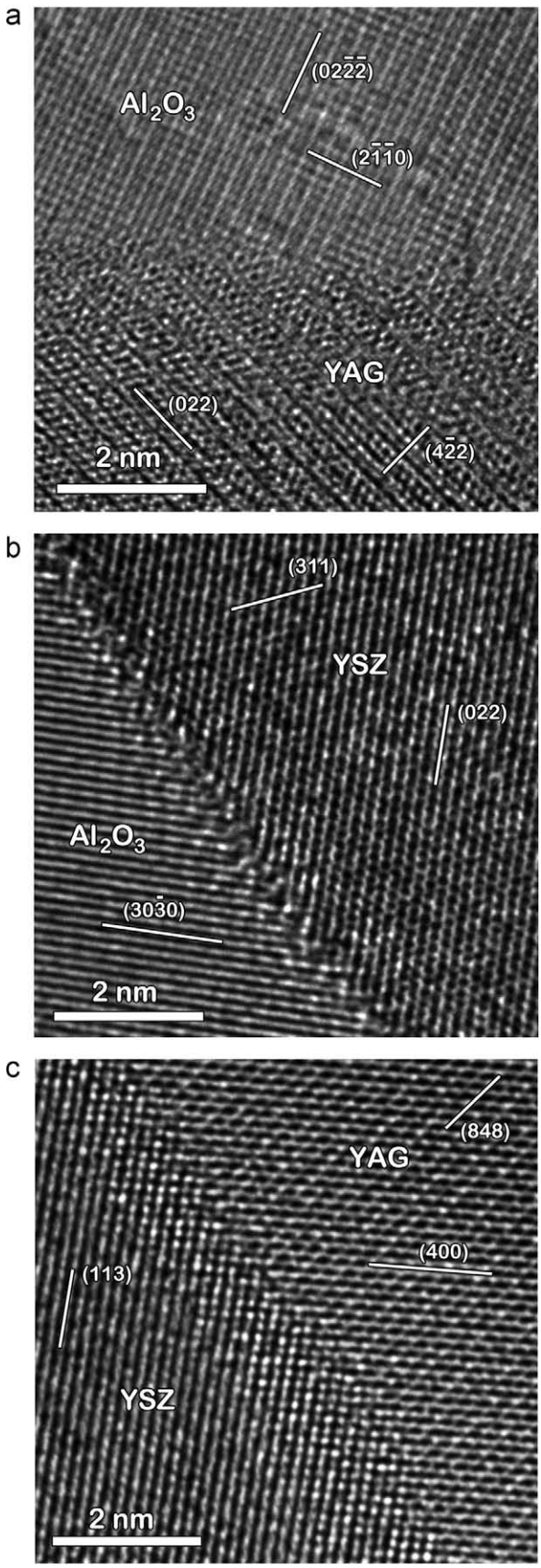

Fig. 5. HRTEM images of the three different interfaces in the ternary eutectic in the as processed condition. (a) Al_2O_3–YAG. (b) Al_2O_3–YSZ. (c) YAG–YSZ. The main atomic planes are marked in the figures.

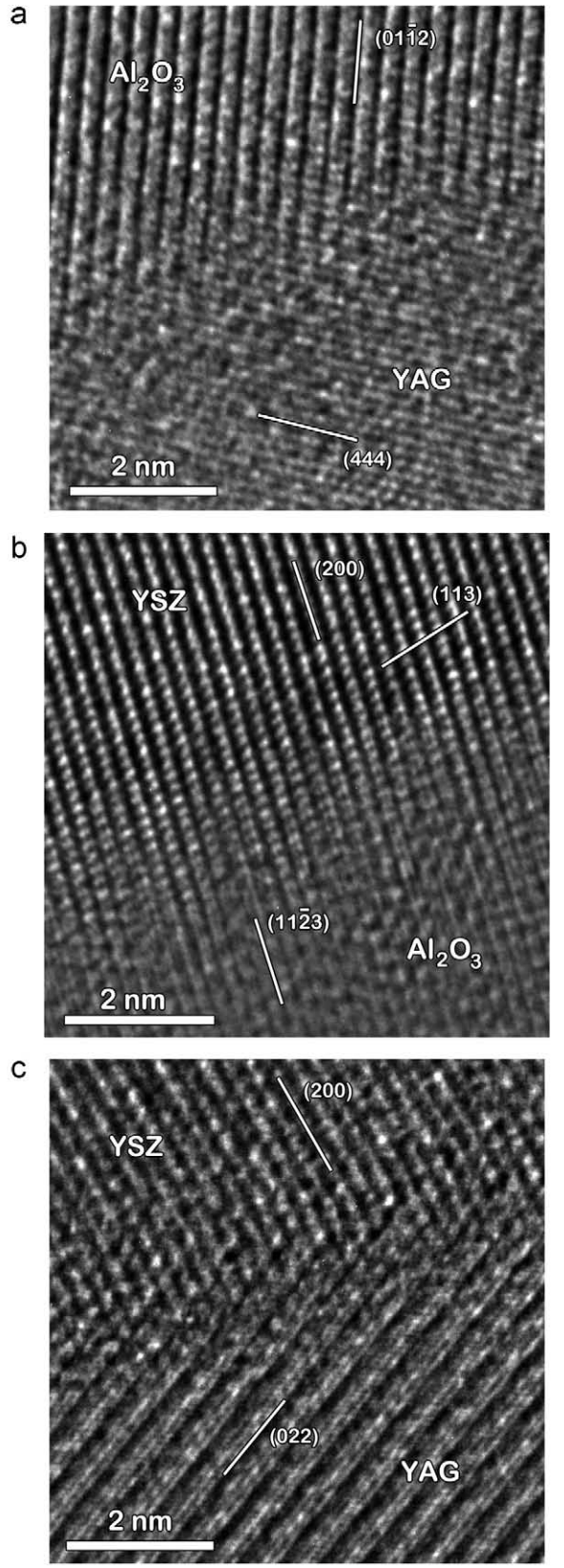

Fig. 6. HRTEM images of the three different interfaces in the ternary eutectic after testing. (a) Al_2O_3–YAG. (b) Al_2O_3–YSZ. (c) YAG–YSZ. The images correspond to the superplastically deformed region. The main atomic planes are marked in the figures.

4. Discussion

Previous evidence of plastic deformation in directionally solidified binary eutectics (Al_2O_3–$GdAlO_3$, Al_2O_3–YAG, Al_2O_3–EAG)[9,13,14] reported continuous flow at higher temperatures (above 1823 K) with creep exponents of around 5. These results were supported by TEM studies, which showed evidence of dislocation activity in both phases, particularly in Al_2O_3. Creep tests between 1673 K and 1823 K in these binary as well as ternary systems (Al_2O_3–YAG–YSZ and Al_2O_3–EAG–YSZ)[13,22–25] with an interpenetrating microstructure reported creep exponents in the range 2–5, which were indicative of creep due to dislocation movement. In general, the creep resistance of the binary Al_2O_3–YAG and Al_2O_3–EAG eutectics was very good, comparable to that of *c*-axis sapphire.[14] The creep exponent decreased with the domain size,[25] indicating that the contribution of bulk diffusion to the overall creep rate increased for finer microstructures. TEM studies provided evidence of dislocation activity in Al_2O_3 but not in EAG[23] or YAG.[22] More detailed studies showed the presence of dislocation networks formed by basal dislocations in Al_2O_3, while the dislocation density in YAG was much lower.[25] It should be noticed that the total (compressive) creep strain in the binary eutectics was always limited (in the range 5–15%) and that these values were even smaller in the case of ternary eutectics[25] in which damage occurred at smaller strains (3–4%).

Dislocation activity was not found in any of the three phases of the nanofibrillar eutectic. This was not expected in the case of YAG because temperatures in excess of 1800 K are necessary to activate dislocation motion in this oxide.[26] YAG has a bcc lattice (lattice constant of ≈1.2 nm) with Y^{3+} ions occupying cubic sites while the smaller Al^{3+} ions are located at both octahedral and tetrahedral sites. The most favorable slip system is $(1\,\bar{1}\,1)\ \langle 1\,1\,1\rangle$ with a very large Burgers vector ($1/2\langle 1\,1\,1\rangle = 1.04$ nm), which mainly accounts for the exceptional creep resistance. In the case of Al_2O_3, plastic deformation mainly occurs by basal slip and, to a lesser extent and higher temperature, by prism plane slip.[27] The Schmid factor for both basal and prismatic slip was zero, however, because the rods were textured and the *c*-axis of sapphire was parallel to the longitudinal stresses induced by bending. Although pyramidal and rhombohedral slip have also been reported in Al_2O_3, the stresses required are too high to be active in the ternary eutectic rods.[27,28] Finally, it should be noticed that dislocation slip is far easier in YSZ than in either Al_2O_3 or YAG[29] but the small thickness of YSZ domains (<50 nm) leads to very high stresses for dislocation nucleation[30] and hinders the dislocation activity in this phase.

Neither interface sliding nor dislocation activity were found operative in the case of nanofibrillar ternary eutectics loaded along the *c*-axis of the Al_2O_3 domains and the large plastic deformations have to be attributed to mass transport by diffusion. This hypothesis is favored by the small dimensions of the domains in the microstructure and is in agreement with the experimental results in Fig. 2b which show that superplastic deformation is enhanced by high temperatures and low strain rates (Fig. 2b). These results are in contrast with those reported in Al_2O_3-based binary and ternary eutectics with interpenetrating microstructure in which dislocation slip in Al_2O_3 was the mechanisms controlling creep deformation below 1800 K. The change in the deformation mechanisms between these materials and nanofibrillar eutectics have to be traced to the microstructural difference (domain size, shape, orientation), which inhibit the activation of basal slip, the easiest slip system in Al_2O_3, in the nanofibrillar eutectics.

Diffusion-controlled creep, which takes place with very low stress exponents (≈1), is a necessary condition to achieve the superplastic behavior but it is not sufficient. An adequate interface strength, relative to the flow stress, is required to mitigate interface cracking and/or cracking during large strain deformation, while coarsening of the fine superplastic microstructure should be inhibited.[31] These conditions, which lead to complex microstructural design rules to obtain ceramics with superplastic behavior, arise naturally by self-assembly upon directional solidification from the melt at very high growth rates. Directional growth of eutectic mixtures ensures low-energy interfaces without glassy phases and very high strength, while they present an excellent resistance to homogeneous coarsening even at temperatures approaching the eutectic point.[10,32] Moreover, superplastic behavior was also found in high purity tetragonal ZrO_2 polycrystals (TZP) and SiO_2-doped TZP with average grain sizes of 0.41 μm and 0.21 μm, respectively.[33] HRTEM showed that the grain boundaries in both materials were free of glassy phases and SiO_2 glass pockets were concentrated at the grain boundary multiple junctions in the second material. These authors reported that segregation of both Y and Si at the grain boundaries strengthened the chemical bonding at the grain boundaries and it was assumed that grain boundary cavitation and resultant fracture was suppressed by the formation of strong grain boundaries.[33] A similar mechanism can be responsible for the superplastic behavior of ternary Al_2O_3–YAG–YSZ eutectics, which are known to present very strong domain boundaries. Finally, it should be noted that the crack deflection mechanism – which enhances the damage tolerance of the ternary eutectic upon tensile deformation – is also important from the viewpoint of manufacturing components with complex shape by means of sheet forming, extrusion, forging, etc. in the superplastic regime.

5. Conclusions

The possibility of superplastic deformation has been demonstrated for the first time in directionally solidified eutectic oxides grown from the melt. Superplastic deformation comes about as a result of a number of features that arise during eutectic solidification at very high growth rates: a nanofibrillar microstructure whose texture impedes deformation by dislocation slip when stressed along the solidification direction, very high interface strength and resistance to homogenous coarsening during high temperature exposure. This finding, together with the high strength and toughness of this nanofibrillar eutectic,[16] has major implications in the manufacturing of eutectic oxides for high temperature structural applications.

Acknowledgements

The financial support from the Spanish Government under grant MAT 2009-13979, by the European Community under project ENSEMBLE NMP4-SL-2008-213669 and by the Comunidad de Madrid through the program ESTRUMAT-CM (S2009/MAT-1585) is gratefully acknowledged. Authors acknowledge the use of Servicio de Microscopia Electrónica (SAI-University of Zaragoza).

References

1. Wiederhorn SM, Hockey BJ, French JD. Mechanisms of deformation of silicon nitride and silicon carbide at high temperatures. *J Eur Ceram Soc* 1999;**19**:2273–84.
2. Guo SQ. Densification of ZrB_2-based composites and their mechanical and physical properties: a review. *J Eur Ceram Soc* 2009;**29**:995–1011.
3. Marshall DB, Cox BN. Integral textile ceramic structures. *Annu Rev Mater Res* 2008;**38**:425–43.
4. Yamamoto H, Akiyama K, Murakami Y. Densification behaviors and high-temperature characteristics of Si_3N_4 sintered bodies using Al_2O_3–Yb_2O_3 additives. *J Eur Ceram Soc* 2006;**26**:1059–67.
5. LLorca J, Elices M, Celemín JA. Toughness and microstructural degradation at high temperature in SiC fiber-reinforced ceramics. *Acta Mater* 1998;**46**:2441–53.
6. More KL, Tortorelli PF, Ferber MK, Keiser JR. Observations of accelerated silicon carbide recession by oxidation at high water-vapor pressures. *J Am Ceram Soc* 2000;**83**:211–3.
7. Hirano K. Application of eutectic composites to gas turbine system and fundamental fracture properties up to 1700 °C. *J Eur Ceram Soc* 2005;**25**:1191–9.
8. Otsuka A, Waku Y, Tanaka R. Corrosion of a unidirectionally solidified Al_2O_3/YAG eutectic composite in a combustion environment. *J Eur Ceram Soc* 2005;**25**:1269–74.
9. Waku Y, Nakagawa T, Wakamoto T, Ohtsubo K, Shimizu K, Kohtoku Y. A ductile ceramic eutectic composite with high strength at 1,873 K. *Nature* 1997;**389**:49–52.
10. LLorca J, Orera VM. Directionally solidified eutectic ceramic oxides. *Prog Mater Sci* 2006;**51**:711–809.
11. Pastor JY, LLorca J, Salazar A, Oliete PB, de Francisco I, Peña JI. Mechanical properties of melt-grown alumina–yttrium aluminum garnet eutectics up to 1900 K. *J Am Ceram Soc* 2005;**88**:1488–95.
12. Mesa MC, Oliete PB, Orera VM, Pastor JY, Martín A, LLorca J. Microstructure and mechanical properties of Al_2O_3/$Er_3Al_5O_{12}$ eutectic rods grown by the laser-heated floating zone method. *J Eur Ceram Soc* 2011;**31**:1241–50.
13. Martinez-Fernandez J, Sayir A, Farmer SC. High-temperature creep deformation of directionally solidified Al_2O_3/$Er_3Al_5O_{12}$. *Acta Mater* 2003;**51**:1705–20.
14. Harada Y, Suzuki T, Hirano K, Waku Y. Ultra-high temperature compressive creep behavior of an in-situ Al_2O_3 single-crystal/YAG eutectic composite. *J Eur Ceram Soc* 2004;**24**:2215–22.
15. Pastor JY, LLorca J, Martín A, Peña JI, Oliete PB. Fracture toughness and strength of Al_2O_3–$Y_3Al_5O_{12}$ and Al_2O_3–$Y_3Al_5O_{12}$–ZrO_2 directionally-solidified eutectic oxides up to 1900K. *J Eur Ceram Soc* 2008;**28**:2345–51.
16. Oliete PB, Peña JI, Larrea A, Orera VM, LLorca J, Pastor JY, Martín A, Segurado J. Ultra-high strength nanofibrillar Al_2O_3–YAG–YSZ eutectics. *Adv Mater* 2007;**19**:2313–8.
17. Pardo JA, Merino RI, Orera VM, Peña JI, González C, Pastor JY, LLorca J. Piezospectroscopic study of residual stresses in Al_2O_3–ZrO_2 eutectic crystals. *J Am Ceram Soc* 2000;**83**:2745–52.
18. Dickey EC, Dravid VP, Hubbard CR. Interlamellar residual stresses in single grains of NiO–ZrO_2(cubic) directionally solidified eutectics. *J Am Ceram Soc* 1997;**80**:2773–80.
19. Lee JH, Yoshikawa A, Fukuda T, Waku Y. Growth and characterization of Al_2O_3/$Y_3Al_5O_{12}$/ZrO_2 ternary eutectic fibers. *J Cryst Growth* 2001;**231**:115–20.
20. Peña JI, Larsson M, Merino RI, de Francisco I, Orera VM, LLorca J, Pastor JY, Martín A, Segurado J. Processing, microstructure and mechanical properties of directionally-solidified Al_2O_3–$Y_3Al_5O_{12}$–ZrO_2 ternary eutectics. *J Eur Ceram Soc* 2006;**26**:3113–21.
21. Iwasa M, Bradt RC. In: Kingery WD, editor. Structure and properties of MgO and Al_2O_3 ceramics. American Ceramic Society; 1984. p. 767–79.
22. Ramírez-Rico J, Pinto-Gómez AR, Martínez-Fernández J, de Arellano López AR, Oliete PB, Peña JI, Orera VM. High temperature plastic behavior of Al_2O_3–$Y_3Al_5O_{12}$ directionally solidified eutectics. *Acta Mater* 2006;**54**:3107–16.
23. Parthasarathy TA, Mah TL, Matson LE. Deformation behavior of an Al_2O_3–$Y_3Al_5O_{12}$ eutectic composite in comparison with sapphire and YAG. *J Am Ceram Soc* 1993;**76**:29–32.
24. Ramírez-Rico J, Pinto-Gómez AR, Martínez-Fernández J, de Arellano López AR, Orera VM, Merino RI, Peña JI. High temperature creep deformation of Al_2O_3-based eutectic ceramics grown by the laser heated float zone method. *Ceram Eng Sci Proc* 2006;**27**:101.
25. Mazerolles L, Perriere L, Lartigue-Korinek S, Parlier M. Creep behavior and related structural defects in Al_2O_3–Ln_2O_3 (ZrO_2) directionally solidified eutectics (Ln = Gd, Er, Y). *J Eur Ceram Soc* 2011;**31**:1219–25.
26. Blumenthal WR, Phillips DS. High-temperature deformation of single-crystal yttrium–aluminum garnet (YAG). *J Am Ceram Soc* 1996;**79**:1047–52.
27. Lagerloff KPD, Heuer AH, Castaing J, Rivière JP, Mitchell TE. Slip and twinning in sapphire α-Al_2O_3. *J Am Ceram Soc* 1994;**77**:385–97.
28. Castillo Rodriguez M, Castaing J, Munoz A, Veyssières P, Domínguez A. Analysis of a kink pair model applied to a peierls mechanism in sapphire α-Al_2O_3 deformed between 200 °C and 1800 °C. *J Am Ceram Soc* 2008;**91**:1612–7.
29. Gómez-García D, Martínez-Fernández J, Domínguez-Rodríguez A, Castaing J. Mechanisms of high-temperature creep of fully stabilized zirconia single crystals as a function of the yttria content. *J Am Ceram Soc* 1997;**80**:1668–72.
30. Brandl C, Derlet PM, Van Swygenhowen H. Dislocation mediated plasticity in Al: the strongest size. *Modell Simul Mater Sci Eng* 2011;**19**:074005.
31. Chen IW, Xue LA. Development of superplastic structural ceramics. *J Am Ceram Soc* 1990;**73**:2585–609.
32. Park DY, Yang JM, Collins JM. Coarsening of lamellar microstructures in directionally solidified yttrium aluminate/alumina eutectic fiber. *J Am Ceram Soc* 2001;**84**:2991–6.
33. Ikuhara Y, Thavorniti P, Sakuma T. Solute segregations at grain boundaries in superplastic SiO_2-doped TZP. *Acta Mater* 1997;**45**:5275–84.